Acta Cryst C STRUCTURAL CHEMISTRY

ISSN 2053-2296

Room-temperature crystal structures of $[CH(NH_2)_2]_3Sb_2X_9$ (X = Br and I)

Prajna Bhatt,[a,b]* Yuhan Liu,[a,c] Anna Regoutz[a,d] and Robert G. Palgrave[a]*

[a]Department of Chemistry, University College London, 20 Gordon St, London, WC1H 0AJ, United Kingdom, [b]Istituto Officina dei Materiali (IOM)–CNR, Area Science Park, S.S.14, Km 163.5, Trieste I-34149, Italy, [c]The Electrochemical Innovation Lab, Department of Chemical Engineering, University College London, Torrington Place, London, WC1E 7JE, United Kingdom, and [d]Department of Chemistry, University of Oxford, Inorganic Chemistry Laboratory, South Parks Road, Oxford, OX1 3QR, United Kingdom. *Correspondence e-mail: bhatt@iom.cnr.it, r.palgrave@ucl.ac.uk

Received 18 November 2025
Accepted 26 January 2026

Edited by M. Yousufuddin, University of North Texas at Dallas, USA

Keywords: halide perovskite; crystallography; counter diffusion crystal growth; CDCG; single crystal; crystal structure; formamidinium; antimony.

CCDC references: 2501007; 2500813

Supporting information: this article has supporting information at journals.iucr.org/c

Crystals of formamidinium antimony, halides, $FA_3Sb_2X_9$ {FA = $[CH(NH_2)_2]^+$; X = Br^- and I^-} {or triformamidinium nonahalidodiantimony, $(CH_5N_2)_3[Sb_2X_9]$}, have been synthesized using a counter diffusion crystal growth (CDCG) method in silica gel and their structures determined from single-crystal X-ray diffraction data. $FA_3Sb_2Br_9$ belongs to the trigonal space group $P\bar{3}m1$, which is known as the $Cs_3Bi_2Br_9$ structure type, and $FA_3Sb_2I_9$ belongs to the hexagonal space group $P6_3/mmc$, called the $Cs_3Cr_2Cl_9$ structure type. The change of the anion type from bromide to iodide results in the change of the structure type and the connectivity of the Sb—X octahedra. These structures are described and compared to the crystal types known for vacancy-ordered triple-perovskites.

1. Introduction

The $A_3B_2X_9$ structure, where A is a monovalent cation, B is a trivalent cation and X is a halide, are commonly described as derivatives of the ABX_3 perovskite structure type. In the ABX_3 form, all $[BX_6]^{3-}$ octahedra are corner-sharing and an $A_3B_2X_9$ compound can be considered similarly, with removal of a third of the B-site cations (Hodgkins *et al.*, 2019; Chang *et al.*, 2016). As such, these structures are more commonly known as vacancy-ordered triple-perovskites. Typical $A_3B_2X_9$ compounds are group 15 halides, mostly comprising of bismuth (Bi) and antimony (Sb) B-sites. The triple-perovskites are considered as perovskite derivatives that can similarly be applied in photovoltaic and radiation detection applications as lead-free alternatives (Eperon *et al.*, 2014; Hao *et al.*, 2014). Due to the optical and electronic properties possessed by these compounds for such applications, materials design approaches also include the formation of compounds with organic monovalent cations. Here, the crystal structure of two organic–inorganic triple-perovskites, namely, $FA_3Sb_2X_9$ {FA = $[CH(NH_2)_2]^+$; X = Br^- and I^-}, are reported.

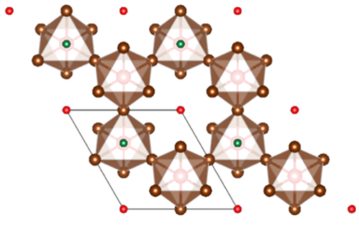

2. Experimental methods

Single crystals were synthesized using a counter diffusion crystal growth (CDCG) method in silica gel. 27 mmol of Sb_2O_3 (Sigma–Aldrich, 99%) were reacted with excess HX, where X = Br (Sigma–Aldrich, 48 wt%) or I (Sigma–Aldrich, 57 wt%), to produce SbX_3 in an acidic solution. In parallel, a 0.6 M aqueous solution of Na_2SiO_3 (Sigma–Aldrich) was prepared using distilled water. The Na_2SiO_3 solution was added dropwise in the presence of vigorous stirring to SbX_3 in a 1:1 (v/v)

Table 1
Experimental details.

Experiments were carried out at 295 K using an Agilent SuperNova Dual Source diffractometer with a HyPix-Arc 100 detector. Absorption was corrected for by multi-scan methods (*CrysAlis PRO*; Rigaku OD, 2022). Refinement was on 19 parameters. H-atom parameters were not defined.

	$FA_3Sb_2Br_9$	**$FA_3Sb_2I_9$**
Crystal data		
Chemical formula	$(CH_5N_2)_3[Sb_2Br_9]$	$(CH_5N_2)_3[Sb_2I_9]$
M_r	998.72	1421.63
Crystal system, space group	Trigonal, $P\bar{3}m1$	Hexagonal, $P6_3/mmc$
a, b, c (Å)	8.5161 (4), 8.5161 (4), 10.0380 (4)	8.7552 (4), 8.7552 (4), 21.8474 (12)
α, β, γ (°)	90, 90, 120	90, 90, 120
V (Å^3)	630.46 (6)	1450.32 (15)
Z	1	2
Radiation type	Cu $K\alpha$	Mo $K\alpha$
μ (mm^{-1})	33.54	11.42
Crystal size (mm)	0.19 × 0.15 × 0.04	0.13 × 0.13 × 0.09
Data collection		
T_{min}, T_{max}	0.061, 1.000	0.263, 1.000
No. of measured, independent and observed $[I > 2\sigma(I)]$ reflections	13069, 546, 391	36967, 896, 456
R_{int}	0.089	0.104
$(\sin\theta/\lambda)_{max}$ (Å^{-1})	0.631	0.728
Refinement		
$R[F^2 > 2\sigma(F^2)]$, $wR(F^2)$, S	0.067, 0.241, 1.14	0.056, 0.242, 1.05
No. of reflections	546	896
No. of restraints	0	1
$\Delta\rho_{max}$, $\Delta\rho_{min}$ (e Å^{-3})	1.11, −1.03	1.24, −0.45

Computer programs: *CrysAlis PRO* (Rigaku OD, 2022), *SHELXT2014* (Sheldrick, 2015*a*), *SHELXL2025* (Sheldrick, 2015*b*), *OLEX2* (Dolomanov *et al.*, 2009), *VESTA* (Momma & Izumi, 2011) and *OLEX2* (Dolomanov *et al.*, 2009).

ratio to form a SbX_3-based silica gel. The solution was allowed to set in 50 ml tall-form beakers in a low-temperature oven at 29 °C over 24 h. Post gelation, solutions containing 41 mmol of FAX {FA = $[CH(NH_2)_2]^+$}, made by dissolving formamidine acetate (Sigma–Aldrich, ≥ 98%) in HX, were added carefully atop the gel using pipettes to avoid disrupting the surface of the gel. The beaker was wrapped with parafilm and placed in an oven. Crystal growth occurred between 2–7 d. $FA_3Sb_2Br_9$ was isolated in the form of pale-yellow plate-like crystals, while $FA_3Sb_2I_9$ crystallized in the morphology of red–brown needle-like crystals (Fig. S1).

Powder X-ray diffraction (PXRD) was measured with a Stoe STADI-P X-ray diffractometer in thin foil transmission (Debye–Scherrer geometry) mode equipped with a germa-

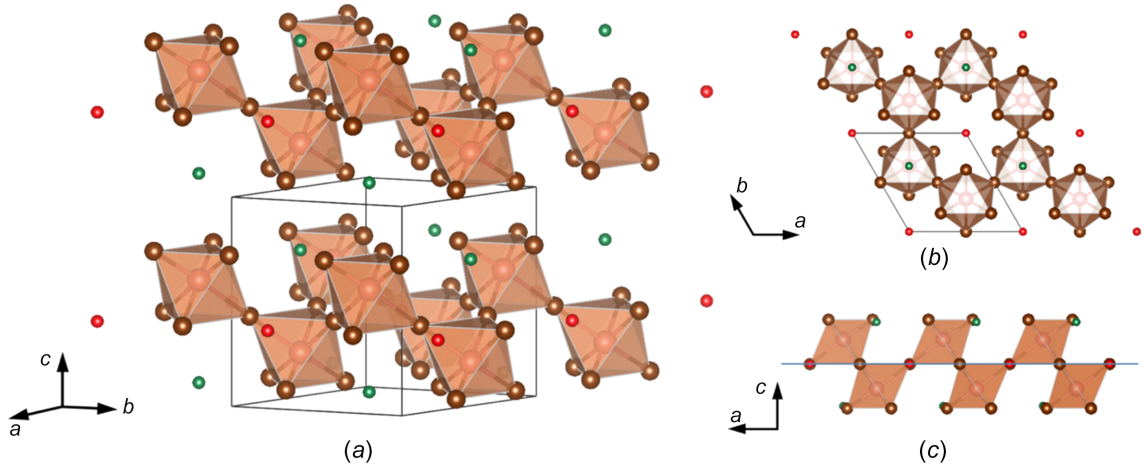

Figure 1
Representation of $FA_3Sb_2Br_9$ from this work shown (*a*) obliquely, (*b*) down the *c* axis and (*c*) down the *b* axis. Four unit cells are shown, with a black-bordered box around one unit cell. Pink spheres represent Sb, brown spheres represent Br and the light-brown octahedra represent the $[SbBr_6]^{3-}$ coordination environment. *A*-site atoms are bifurcated by their Wyckoff positions, *i.e.* green spheres represent C atoms on site 2*d* between $[SbBr_6]^{3-}$ layers and red spheres reside on site 1*a* between rings of six $[SbBr_6]^{3-}$ octahedra. C atoms are used in place of the FA ion, as explained in the text. The blue layer in (*c*) represents the common plane of bromide ions, as explained in the text. The figure was prepared using the *VESTA* software suite (Version 3; Momma & Izumi, 2011).

nium (111) monochromator and a Dectris Mythen 1K detector, with Cu $K\alpha$ (λ = 1.5406 Å, using 40 kV and 30 mA) radiation at 298 K. Samples were loaded between two clear acetate sheets and sealed using silicon vacuum grease. Diffraction patterns were collected in a 2θ range from 2 to 70°, with a step size of 0.015° and a scan rate of 5 s per step. Rietveld refinement models (Rietveld, 1966) on PXRD data were carried out within the *TOPAS-Academic* software suite (Version 7; Coelho, 2018; Coelho, 2022).

Single-crystal X-ray diffraction (SCXRD) was performed using an Agilent SuperNova diffractometer with an Atlas CCD detector. Full spheres of data were collected using 1° scan frames in ω with monochromated Cu or Mo $K\alpha$ radiation at 295 K. A refinement of the positions of the C, N and H atoms was not carried out because isotropic rotation of the FA cations takes place at room temperature like other organic monovalent cations (Liu *et al.*, 2022). The supporting information includes a discussion on the treatment of the FA cation in detail. The experimental details from SCXRD are summarized in Table 1.

All other experimental techniques employed (Raman spectroscopy, X-ray photoelectron spectroscopy and diffuse reflectance spectroscopy) are described in the supporting information.

3. Results and discussion

3.1. Description of structures

3.1.1. Formamidinium antimony bromide, $FA_3Sb_2Br_9$

$FA_3Sb_2Br_9$ was found to crystallize in the $Cs_3Bi_2Br_9$ structure type. Compounds of this crystal type belong to the trigonal space group $P\bar{3}m1$ (Lazarini, 1977). The lattice parameters for $FA_3Sb_2Br_9$ are a = 8.5161 (4), c = 10.0380 (4) Å and V = 630.46 (6) Å^3. Similar to most organic–inorganic triple-perovskites, the FA cations possess rotational disorder at room temperature (Bhatt *et al.*, 2025), resulting in failed attempts to localize discrete C and N atoms. The solvent-masking routine in *OLEX2* was employed (Dolomanov *et al.*, 2009) and a void volume of 244 Å^3 per unit cell identified (38.7% of the total unit cell). The integrated electron count within this void was found to be 77 electrons. This is in excellent agreement with the 75 electrons expected theoretically for the three FA cations in the unit cell, confirming the existence of FA cations in the compound. In this article, a single C atom was used as a placeholder in the unit cell to represent the FA cation, as discussed in the methods and supporting information.

Common bromide-based vacancy-ordered triple-perovskites that are also known to crystallize in this structure type include $MA_3Bi_2Br_9$, $MA_3Sb_2Br_9$ and $FA_3Bi_2Br_9$ (MA = $CH_3NH_3^+$) (Ishihara *et al.*, 1992; Tomaszewski, 1994; Shen *et al.*, 2020). The isostructural $Cs_3Bi_2Br_9$ was reported to have the Cs and Br atoms in a cubic close-packed arrangement, with the Bi atom occupying one-sixth of the octahedral holes in the crystal structure. The structure of $FA_3Sb_2Br_9$ can also be considered a '2D form' of a vacancy-ordered triple-perovskite (Chen *et al.*, 2024). Here, the corner-sharing $[SbBr_6]^{3-}$ octahedra possess a structural dimensionality such that the octahedra can be described as 2D layers, within which *A*-site cations are located. For $FA_3Sb_2Br_9$ visualized in Fig. 1(*a*), $[SbBr_6]^{3-}$ octahedra (in light brown) generate these 2D layers by sharing three Br atoms with three different neighbouring octahedra.

Within the layer, the corner-sharing octahedra result in the formation of six-connected octahedra 'rings' [Fig. 1(*b*)] where the FA ions reside (red atoms). This is similar to the ABX_3 perovskite structure with the exception of six surrounding *B*-site octahedra rather than eight (Xia *et al.*, 2020). In addition, the FA ions fill spaces between these corner-sharing octahedra 2D layers (green), observed as $[SbBr_6]^{3-}$–FA^+–$[SbBr_6]^{3-}$ layers along the *c* axis. The *A*- and *B*-site coordination numbers are 12 and 6, respectively, and agree with other compounds that crystallize in this structure type.

This structure has also been described previously as isolated layers formed by $[SbBr_6]^{3-}$ octahedra pointing alternatively

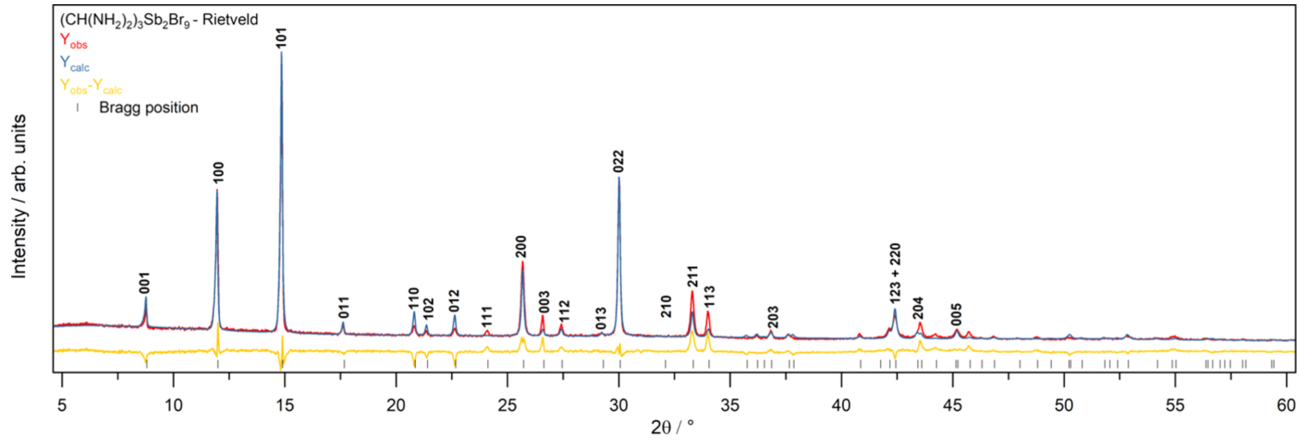

Figure 2
Rietveld refinement on the PXRD pattern of $FA_3Sb_2Br_9$ single crystals made by CDCG. Input unit-cell information was taken from the structure resolved from SCXRD data. Y_{obs} (red) is the collected diffraction pattern, Y_{calc} (blue) is the calculated pattern from *TOPAS-Academic* and $Y_{obs} - Y_{calc}$ (yellow) is the residual plot. Reflections that are ≥5% of the highest intensity reflection are indexed.

up or down with respect to a plane of common halide atoms (Tomaszewski, 1994). Fig. 1(*c*) shows the orientation of the octahedra alternating in orientation with respect to the layer of bromide ions (displayed with a blue line).

Refined atomic position parameters, selected interatomic distances and bond angles for $FA_3Sb_2Br_9$ are listed in Table 2. Each $[SbBr_6]^{3-}$ octahedron has three equivalent Sb—Br1 and Sb—Br2 distances of 3.0598 (7) and 2.612 (2) Å, respectively. These are comparable to the distances reported in $MA_3Sb_2Br_9$, where Sb—Br1 = 3.000 Å and Sb—Br2 = 2.627 Å (Ishihara *et al.*, 1992). Both $FA_3Sb_2Br_9$ and $MA_3Sb_2Br_9$ have similar bond angles of Br1—Sb—Br2 (≈177°) and Br*x*—Sb—Br*x* (in the range 88–92°), where *x* is the same number. This difference in the Sb—Br bond lengths and angles within a single octahedron arises from the distortions from the vertex-sharing Br1 halide ions.

When compared to the bismuth compound $MA_3Bi_2Br_9$, the Sb—Br1 distance of $FA_3Sb_2Br_9$ is similar to Bi—Br1 (3.054 Å), while Sb—Br2 of $FA_3Sb_2Br_9$ is smaller than Bi—Br2 (2.772 Å) in $MA_3Bi_2Br_9$. The six-coordinate ionic radius of Sb^{3+} (0.76 Å) in $FA_3Sb_2Br_9$ is smaller compared to that of Bi^{3+} (1.03 Å) in $MA_3Bi_2Br_9$ (Ahrens, 1952; Shannon, 1976). Antimony compounds are therefore expected to have smaller unit cells and shorter bond lengths compared to bromobismuthates. Smaller *B*-site ions also mean the $[SbBr_6]^{3-}$ octahedra are expected to have lower angular distortions than $[BiBr_6]^{3-}$. Considering bond angles, there is a stronger distortion of the Br—Bi—Br angles, with Br1—Bi—Br2 being ≈169.3° and Br*x*—Bi—Br*x* in the range 84–88°. The angles in the Bi compound are smaller than equivalent octahedral bond angles in $FA_3Sb_2Br_9$, where Br atoms are arranged around a larger cation (Lazarini, 1977).

Table 2
Atomic position parameters, interatomic distances (Å) and bond angles (°) obtained from the structural solution of SCXRD data collected at 295 K of $FA_3Sb_2Br_9$.

x, *y* and *z* are the position parameters of different atoms, and 'Occ' is the occupancy of the atom at the determined position. W is the Wyckoff position notation and *U* is the anisotropic displacement parameter. C atoms are used in place of the FA ion, as explained in the text. Bond distances and angles were determined using the *VESTA* software suite (Version 3; Momma & Izumi, 2011).

Atom	*x*	*y*	*z*	Occ	W	*U*
Sb	1/3	2/3	0.31852 (12)	1	2*d*	0.1112 (8)
Br1	1/2	3/2	1/2	1	3*f*	0.1457 (11)
Br2	0.6278 (3)	0.81392 (16)	0.17401 (18)	1	6*i*	0.1709 (12)
C1	2/3	4/3	0.191 (4)	1	2*d*	0.21 (3)
C2	−3.00000	−1.00000	1/2	1	1*b*	0.22 (3)

Atoms	Interatomic distance	Atoms	Bond angle
Sb—Br1	3.0598 (7)	Br1—Sb—Br2	177.20 (6)
Sb—Br2	2.6119 (19)	Br1—Sb—Br1	88.18 (3)
Br1—Br2	4.016 (3)	Br2—Sb—Br2	92.14 (8)

The plotted Rietveld refinement of PXRD data (Fig. 2) shows excellent agreement between the Y_{obs} and Y_{calc} plots. The commensurate position of the Bragg reflections from SCXRD resolution and the peak positions from PXRD data indicate that the structural resolution is accurate for both single crystals and polycrystalline powders. A goodness-of-fit (GOF) of 1.14 and R_w = 10.319% were achieved.

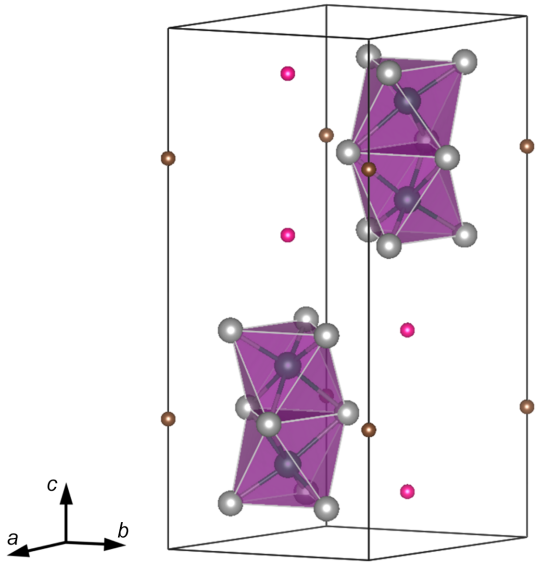

Figure 3
Unit-cell representation of $FA_3Sb_2I_9$ from this work shown obliquely. Green spheres represent Sb, grey spheres represent I and purple bi-octahedra represent the $[Sb_2I_9]^{3-}$ coordination environment. C atoms are bifurcated by their Wyckoff positions, *i.e.* pink spheres represent C atoms on site 4*f* and brown spheres reside on site 2*b*. C atoms are used in place of the FA ion, as explained in the text. The figure was prepared using the *VESTA* software suite (Version 3; Momma & Izumi, 2011).

3.1.2. Formamidinium antimony iodide, $FA_3Sb_2I_9$

$FA_3Sb_2I_9$ belongs to the hexagonal space group $P6_3/mmc$ at room temperature. This is known as the $Cs_3Cr_2Cl_9$ structural type wherein $FA_3Bi_2I_9$, $MA_3Sb_2I_9$ (MA = CH_3NH_3), $Cs_3Sb_2I_9$ and $Cs_3Bi_2I_9$ are known structures of group 15 triple-perovskites (Szklarz *et al.*, 2019; Ju *et al.*, 2018; Yamada *et al.*, 1997; Arakcheeva *et al.*, 1999). $FA_3Sb_2I_9$ has been reported previously at 195 K, also exhibiting the space group $P6_3/mmc$ (Szklarz *et al.*, 2020). One way to describe this structure considers the FA cation and I atoms forming close-packed FAI_3 layers, with Sb atoms occupying one-sixth of the total octahedral holes (Arakcheeva *et al.*, 1999). The close packing of the *AX* layers is hexagonal and the layered structure is comprised of isolated $[Sb_2I_9]^{3-}$ bioctahedra or 'dimers' which share a triangular face and three iodide ions. These are illustrated in Fig. 3 as purple polyhedra. As such, this variant of the triple-perovskite is also regarded as a 0D isolated dimer structure. The Sb—Sb axis within each bioctahedron is parallel to the *c* axis.

As in the bromide structure, the FA cations were found to be highly disordered. A total void volume of 541 $Å^3$ (37.3% of the total unit cell) was identified, containing 105 electrons per unit cell, which corresponds to the region occupied by the disordered cations. While this is lower than the ideal count for six FA cations (150 electrons), it is consistent with the presence of rotationally disordered organic species that

cannot be resolved into discrete atomic positions. When a single C atom in the void replaces one FA cation, a similar *R* factor is achieved. Thus, the FA cations in the unit cell are represented by C atoms.

The C1 position of the cation (pink) at Wyckoff position 4*f* is in the same plane of each dimer and its coordination can be described as identical layered stacking of the iodide ions with a hexagonal coordination (six) on either side of the FA cation (Stranger *et al.*, 1978). Additionally, C2, in brown, appears displaced from the plane of the terminal iodide ions of the bioctahedra, also resulting in a cuboctahedral coordinated FAI_{12} environment.

The atomic positions, bioctahedral bond lengths and angles of $FA_3Sb_2I_9$ are summarized in Table 3. For $FA_3Sb_2I_9$, the Sb—I1 bond length is 3.2323 (12) Å, while Sb—I2 is 2.8758 (13) Å. These align well with the Sb—I bond lengths of the structure that Szklarz *et al.*, (2020) collected on $FA_3Sb_2I_9$ at 195 K, *i.e.* 3.213 and 2.881 Å. These values are also similar to those in the bioctahedra of $A_3Sb_2I_9$ (*A* = Cs or MA), with bond lengths of 3.198 and 2.870 Å for *A* = Cs, and 3.213 and 2.887 Å for *A* = MA (Chabot & Parthé, 1978; Ju *et al.*, 2018). These confirm crystallization of $A_3Sb_2I_9$ in a $Cs_3Cr_2Cl_9$-type crystal structure at room temperature. Bond angles in the range 83–94° for terminal I—Sb—I, and around 172.9° for bridging I—Sb—I are similarly comparable to literature values. For $MA_3Sb_2I_9$, the bond angles are in the range 84–91° for terminal I—Sb—I, and around 173.8° for bridging I—Sb—I. These angles diverge from 90 and 180°, respectively, indicating the distortion of the bioctahedral units as a result of face-sharing in the *ab* plane.

The Rietveld refinement of PXRD data in Fig. 4 is based on the SCXRD structure and shows good agreement with the PXRD data collected, fortifying the triple-perovskite structure at room temperature. A goodness-of-fit (GOF) of 1.11 and R_w = 9.217% were achieved.

X-ray photoelectron spectroscopy (XPS) was employed for the identification of chemical environments and elemental quantification to verify the formation of $A_3B_2X_9$ compounds; see Fig. S2 and Tables S1 and S2 in the supporting information. The elemental quantification in Table S2 matches closely the expected $A_3B_2X_9$ composition. From the survey spectra [Fig. S2(*a*)], core lines from the expected elements for $FA_3Sb_2X_9$ are observed, in addition to Si from contamination during sample plating. The supporting information also reports the absolute binding energy (BE) values of the core levels in Table S1, due to issues noted for the application of charge compensation (such as C 1*s*) for organic–inorganic compounds (Jia *et al.*, 2023). From the XPS spectra, the relative BE (ΔBE) between the N1*s* core line (from the FA cation, appearing around 400 eV) and the Sb $3d_{5/2}$ core line (appearing around 530 eV) is 130.2 eV for $FA_3Sb_2Br_9$ and 129.6 eV for $FA_3Sb_2I_9$. The values are within 1 eV of each other, indicating the presence of similar *A*- and *B*-site chemical environments, regardless of the halide. The reduction in the ΔBE(Sb $3d_{5/2}$—N1*s*) values from $FA_3Sb_2Br_9$ to $FA_3Sb_2I_9$ may be due to a shift of Sb3 $d_{5/2}$ to lower BE and/or a shift of N 1*s* to higher BE. A shift of a core level to lower (higher) BEs is indicative of higher (lower) charge densities around the atom (Greczynski & Hultman, 2022). Given the lower electronegativity of iodine, it is reasonable to assume that the Sb in

Table 3
Atomic position parameters, interatomic distances (Å) and bond angles (°) obtained from the structural solution of SCXRD data collected at 295 K of $FA_3Sb_2I_9$.

See Table 2 for definitions.

Atom	*x*	*y*	*z*	Occ	W	*U*
Sb	2/3	1/3	0.34482 (6)	1	4*f*	0.0810 (6)
I1	0.50288 (8)	0.49712 (8)	1/2	1	6*h*	0.1312 (7)
I2	0.82610 (9)	0.65220 (18)	0.41593 (6)	1	12*k*	0.1312 (7)
C1	1/3	2/3	0.405 (4)	1	4*f*	0.21 (2)
C2	1.00000	1.00000	1/4	1	2*b*	0.20 (3)

Atoms	Interatomic distance	Atoms	Bond angle
Sb—I1	3.2323 (12)	I1—Sb—I2	172.94 (5)
Sb—I2	2.8758 (13)	I1—Sb—I1	83.41 (3)
I1—I2	4.3762 (15)	I2—Sb—I2	93.50 (5)

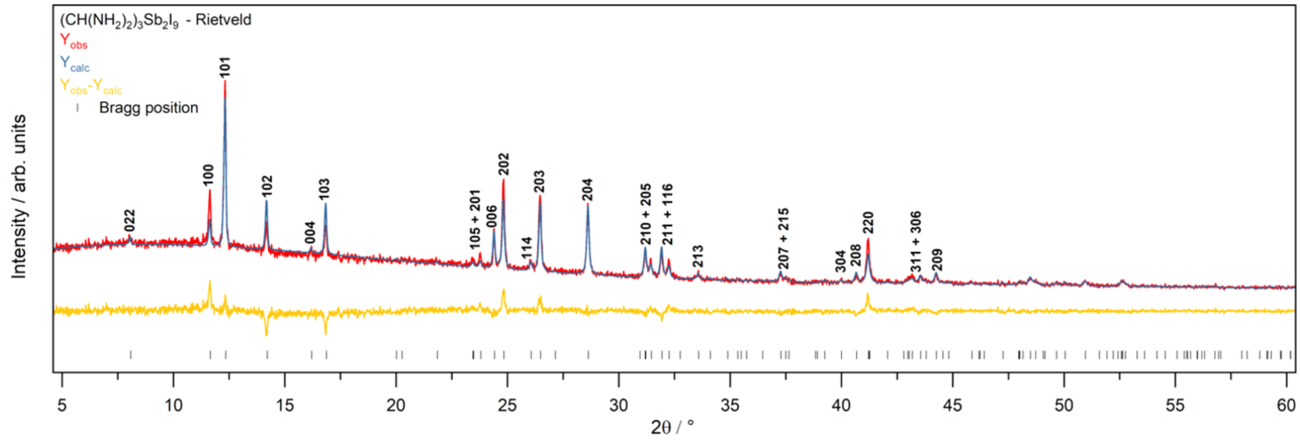

Figure 4
Rietveld refinement on the PXRD pattern of $FA_3Sb_2I_9$ single crystals made by CDCG. Input unit-cell information was taken from the structure resolved from SCXRD data. Y_{obs} (red) is the collected diffraction pattern, Y_{calc} (blue) is the calculated pattern from *TOPAS-Academic* and $Y_{obs} - Y_{calc}$ (yellow) is the residual plot. Reflections that are ≥5% of the highest intensity reflection are indexed.

$FA_3Sb_2I_9$ has greater charge density than Sb in $FA_3Sb_2Br_9$, which then explains the change in ΔBE(Sb $3d_{5/2}$—N 1*s*).

4. Conclusions and future perspectives

Single crystals of $FA_3Sb_2X_9$ (X = Br^- and I^-) were grown successfully by counter diffusion crystal growth in silica gel, and their room-temperature structures identified. $FA_3Sb_2Br_9$ crystallizes in the $Cs_3Bi_2Br_9$ structure type, while $FA_3Sb_2I_9$ belongs to the $Cs_3Cr_2Cl_9$ structure type. Both structures were compared to known compounds of group 15 triple-perovskites. Further work to understand these crystal structures may include the study of temperature-dependent phase transitions, in particular to resolve the organic *A*-site positions and to gain further insights on the stability of these compounds.

5. Related literature

The following references are cited in the supporting information for this article: Kalha *et al.* (2020); McCall *et al.* (2017); Scofield (1973); Scholz *et al.* (2018); Teterin *et al.* (2008); Wolstenholme (2008).

Acknowledgements

XPS was carried out at Harwell XPS, the National XPS Facility (EP/Y023587/1).

Data availability

Data for this article, including all processed data of the figures, are available at Zenodo in Origin format at https://doi.org/10.5281/zenodo.17578603.

References

Ahrens, L. H. (1952). *Geochim. Cosmochim. Acta* **2**, 155–169.
Arakcheeva, A., Bonin, M., Chapuis, G. & Zaitsev, A. (1999). *Z. Kristallogr. Cryst. Mater.* **214**, 279–283.
Bhatt, P., Stucky de Quay, T., Liu, Y., Evans, T., McCullough, O., Fernando, N. K., Kalha, C., Palgrave, R. G. & Regoutz, A. (2025). *ChemPhysChem* **26**, e202500370.
Chabot, B. & Parthé, E. (1978). *Acta Cryst.* B**34**, 645–648.
Chang, J.-H., Doert, T. & Ruck, M. (2016). *Z. Anorg. Allge Chem.* **642**, 736–748.
Chen, C., Xu, J., Wang, X. & Palgrave, R. G. (2024). *J. Mater. Chem. A* **12**, 5055–5079.
Coelho, A. A. (2018). *J. Appl. Cryst.* **51**, 210–218.
Coelho, A. A. (2022). *TOPAS-Academic*. Version 7.1. https://topas-academic.com/.
Dolomanov, O. V., Bourhis, L. J., Gildea, R. J., Howard, J. A. K. & Puschmann, H. (2009). *J. Appl. Cryst.* **42**, 339–341.
Eperon, G. E., Burlakov, V. M., Docampo, P., Goriely, A. & Snaith, H. J. (2014). *Adv. Funct. Mater.* **24**, 151–157.
Greczynski, G. & Hultman, L. (2022). *Vacuum* **205**, 111463.
Hao, F., Stoumpos, C. C., Cao, D. H., Chang, R. P. H. & Kanatzidis, M. G. (2014). *Nat. Photonics* **8**, 489–494.
Hodgkins, T. L., Savory, C. N., Bass, K. K., Seckman, B. L., Scanlon, D. O., Djurovich, P. I., Thompson, M. E. & Melot, B. C. (2019). *Chem. Commun.* **55**, 3164–3167.
Ishihara, H., Watanabe, K., Iwata, A., Yamada, K., Kinoshita, Y., Okuda, T., Krishnan, V., Dou, S.-Q. & Weiss, A. (1992). *Z. Naturforsch. A* **47**, 65–74.
Jia, X., Liu, Y., Bhatt, P., Perry, R. S., Parkin, I. P. & Palgrave, R. G. (2023). *Phys. Chem. Chem. Phys.* **25**, 4563–4569.
Ju, D., Jiang, X., Xiao, H., Chen, X., Hu, X. & Tao, X. (2018). *J. Mater. Chem. A* **6**, 20753–20759.
Kalha, C., Fernando, N. K. & Regoutz, A. (2020). *Digitisation of Scofield Photoionisation Cross Section Tabulated Data, figshare*. Dataset. https://doi.org/10.6084/m9.figshare.12967079.v1.
Lazarini, F. (1977). *Acta Cryst.* B**33**, 2961–2964.
Liu, Y., Cockcroft, J. K., Chen, Z., Hayward, M. A., Henry, P. F., Perry, R. S. & Palgrave, R. G. (2022). *J. Mater. Chem. C* **10**, 11938–11945.
McCall, K. M., Stoumpos, C. C., Kostina, S. S., Kanatzidis, M. G. & Wessels, B. W. (2017). *Chem. Mater.* **29**, 4129–4145.
Momma, K. & Izumi, F. (2011). *J. Appl. Cryst.* **44**, 1272–1276.
Rietveld, H. M. (1966). *Acta Cryst.* **20**, 508–513.
Rigaku OD (2022). *CrysAlis PRO*. Rigaku Oxford Diffraction Ltd, Yarnton, Oxfordshire, England.
Scholz, M., Morgenroth, M., Oum, K. & Lenzer, T. (2018). *J. Phys. Chem. C* **122**, 5854–5863.
Scofield, J. H. (1973). Technical Report UCRL-51326. Lawrence Livermore Laboratory, California, USA.
Shannon, R. D. (1976). *Acta Cryst.* A**32**, 751–767.
Sheldrick, G. M. (2015*a*). *Acta Cryst.* A**71**, 3–8.
Sheldrick, G. M. (2015*b*). *Acta Cryst.* C**71**, 3–8.
Shen, Y., Yin, J., Cai, B., Wang, Z., Dong, Y., Xu, X. & Zheng, H. (2020). *Nanoscale Horiz.* **5**, 580–585.
Stranger, R., Grey, I. E., Madsen, I. C. & Smith, P. W. (1978). *J. Solid State Chem.* **69**, 162–170.
Szklarz, P., Gągor, A., Jakubas, R., Zieliński, P., Piecha-Bisiorek, A., Cichos, J., Karbowiak, M., Bator, G. & Ciżman, A. (2019). *J. Mater. Chem. C* **7**, 3003–3014.
Szklarz, P., Jakubas, R., Gągor, A., Bator, G., Cichos, J. & Karbowiak, M. (2020). *Inorg. Chem. Front.* **7**, 1780–1789.
Teterin, A. Y., Teterin, Y. A., Maslakov, K., Yarzhemskii, V., Sverchkov, S., Denker, B., Galagan, B., Iskhakova, L., Bulatov, L., Dvoirin, V., Mashinskii, V. M., Umnikove, A. A., Gur'yanove, A. N., Nefedovb, V. I. & Dianov, E. M. (2008). *Dokl. Phys.* **53**, 566–570.
Tomaszewski, P. (1994). *Phys. Status Solidi B* **181**, 15–21.
Wolstenholme, J. (2008). *Surf. Interface Anal.* **40.** 966–968.
Xia, M., Yuan, J.-H., Niu, G., Du, X., Yin, L., Pan, W., Luo, J., Li, Z., Zhao, H. K.-H., Xue, X., Miao, X. & Tang, J. (2020). *Adv. Funct. Mater.* **30**, 1910648.
Yamada, K., Sera, H., Sawada, S., Tada, H., Okuda, T. & Tanaka, H. (1997). *J. Solid State Chem.* **134**, 319–325.

supporting information

Acta Cryst. (2026). C**82**, 138-143 [https://doi.org/10.1107/S2053229626000811]

Room-temperature crystal structures of $[CH(NH_2)_2]_3Sb_2X_9$ (X = Br and I)

Prajna Bhatt, Yuhan Liu, Anna Regoutz and Robert G. Palgrave

Computing details

Triformamidinium nonabromidodiantimony (I)

Crystal data

$(CH_5N_2)_3[Sb_2Br_9]$
M_r = 998.72
Trigonal, $P\bar{3}m1$
a = 8.5161 (4) Å
c = 10.0380 (4) Å
V = 630.46 (6) Å^3
Z = 1
$F(000)$ = 435
D_x = 2.630 Mg m^{-3}
Cu $K\alpha$ radiation, λ = 1.54184 Å
Cell parameters from 2382 reflections
θ = 4.4–52.7°
μ = 33.54 mm^{-1}
T = 295 K
Plate, clear yellowish yellow
0.19 × 0.15 × 0.04 mm

Data collection

Agilent SuperNova Dual Source diffractometer with a HyPix-Arc 100 detector
Radiation source: micro-focus sealed X-ray tube, SuperNova (Cu) X-ray Source
Mirror monochromator
Detector resolution: 10.0000 pixels mm^{-1}
ω scans
Absorption correction: multi-scan (CrysAlis PRO; Rigaku OD, 2022)
T_{min} = 0.061, T_{max} = 1.000
13069 measured reflections
546 independent reflections
391 reflections with $I > 2\sigma(I)$
R_{int} = 0.089
θ_{max} = 76.8°, θ_{min} = 4.4°
h = −10→10
k = −10→9
l = −12→12

Refinement

Refinement on F^2
Least-squares matrix: full
$R[F^2 > 2\sigma(F^2)]$ = 0.067
$wR(F^2)$ = 0.241
S = 1.14
546 reflections
19 parameters
0 restraints
Primary atom site location: dual
H-atom parameters not defined
$w = 1/[\sigma^2(F_o^2) + (0.1581P)^2]$ where $P = (F_o^2 + 2F_c^2)/3$
$(\Delta/\sigma)_{max} < 0.001$
$\Delta\rho_{max}$ = 1.11 e Å^{-3}
$\Delta\rho_{min}$ = −1.03 e Å^{-3}

Special details

Geometry. All esds (except the esd in the dihedral angle between two l.s. planes) are estimated using the full covariance matrix. The cell esds are taken into account individually in the estimation of esds in distances, angles and torsion angles; correlations between esds in cell parameters are only used when they are defined by crystal symmetry. An approximate (isotropic) treatment of cell esds is used for estimating esds involving l.s. planes.

Refinement. Data was processed with the *CrysAlis PRO* software suite, and the structure was solved with *SHELXT* (Sheldrick, 2015*a*) and refined with *SHELXL* (Sheldrick, 2015*b*) within the *OLEX2* software suite (Dolomanov *et al.*, 2009).

Fractional atomic coordinates and isotropic or equivalent isotropic displacement parameters (Å²)

	x	*y*	*z*	U_{iso}*/U_{eq}
Sb1	0.3333	0.6667	0.31852 (12)	0.1112 (8)
Br1	0.5000	1.5000	0.5000	0.1457 (11)
Br2	0.6278 (3)	0.81392 (16)	0.17401 (18)	0.1710 (12)
C1	0.6667	1.3333	0.191 (4)	0.21 (3)
C2	0.0000	0.0000	0.5000	0.22 (3)

Atomic displacement parameters (Å²)

	U^{11}	U^{22}	U^{33}	U^{12}	U^{13}	U^{23}
Sb1	0.1230 (10)	0.1230 (10)	0.0876 (9)	0.0615 (5)	0.000	0.000
Br1	0.1652 (19)	0.1652 (19)	0.1377 (19)	0.1057 (19)	−0.0055 (6)	0.0055 (6)
Br2	0.1663 (18)	0.205 (2)	0.1289 (15)	0.0832 (9)	0.0485 (12)	0.0242 (6)
C1	0.20 (3)	0.20 (3)	0.24 (7)	0.101 (17)	0.000	0.000
C2	0.24 (5)	0.24 (5)	0.18 (6)	0.12 (2)	0.000	0.000

Geometric parameters (Å, º)

Sb1—Sb1^{i}	6.1195 (14)	Sb1—Br2^{viii}	2.6119 (19)
Sb1—Sb1^{ii}	6.1195 (14)	Sb1—Br2^{ix}	2.6119 (19)
Sb1—Sb1^{iii}	6.1195 (14)	Sb1—Br2	2.612 (2)
Sb1—Br1^{iv}	3.0598 (7)	Br1—Sb1^{x}	3.0597 (7)
Sb1—Br1^{v}	10.8696 (5)	Br1—Sb1^{ii}	10.8696 (5)
Sb1—Br1^{vi}	3.0598 (7)	Br1—Sb1^{i}	3.0598 (7)
Sb1—Br1^{vii}	3.0598 (7)		
Sb1^{iii}—Sb1—Sb1^{ii}	88.19 (3)	Br2—Sb1—Sb1^{i}	89.80 (4)
Sb1^{i}—Sb1—Sb1^{ii}	88.18 (3)	Br2—Sb1—Sb1^{iii}	177.20 (6)
Sb1^{iii}—Sb1—Sb1^{i}	88.18 (3)	Br2—Sb1—Sb1^{ii}	89.80 (4)
Sb1^{ii}—Sb1—Br1^{v}	89.489 (7)	Br2^{ix}—Sb1—Sb1^{ii}	89.80 (4)
Sb1^{iii}—Sb1—Br1^{v}	122.428 (18)	Br2^{viii}—Sb1—Sb1^{ii}	177.20 (6)
Sb1^{i}—Sb1—Br1^{v}	34.243 (8)	Br2^{ix}—Sb1—Sb1^{i}	177.20 (6)
Br1^{vii}—Sb1—Sb1^{iii}	88.18 (3)	Br2^{ix}—Sb1—Br1^{vii}	177.20 (6)
Br1^{vi}—Sb1—Sb1^{ii}	0.0	Br2—Sb1—Br1^{vi}	89.80 (4)
Br1^{vi}—Sb1—Sb1^{iii}	88.19 (3)	Br2—Sb1—Br1^{v}	55.58 (4)
Br1^{iv}—Sb1—Sb1^{iii}	0.0	Br2^{viii}—Sb1—Br1^{iv}	89.80 (4)
Br1^{vii}—Sb1—Sb1^{i}	0.0	Br2^{viii}—Sb1—Br1^{vii}	89.80 (4)
Br1^{iv}—Sb1—Sb1^{ii}	88.18 (3)	Br2—Sb1—Br1^{iv}	177.20 (6)
Br1^{iv}—Sb1—Sb1^{i}	88.18 (3)	Br2—Sb1—Br1^{vii}	89.80 (4)
Br1^{vi}—Sb1—Sb1^{i}	88.18 (3)	Br2^{ix}—Sb1—Br1^{iv}	89.80 (4)
Br1^{vii}—Sb1—Sb1^{ii}	88.18 (3)	Br2^{ix}—Sb1—Br1^{vi}	89.80 (4)
Br1^{vii}—Sb1—Br1^{vi}	88.18 (3)	Br2^{viii}—Sb1—Br1^{vi}	177.20 (6)
Br1^{vii}—Sb1—Br1^{iv}	88.18 (3)	Br2^{viii}—Sb1—Br1^{v}	89.945 (11)
Br1^{vi}—Sb1—Br1^{v}	89.489 (7)	Br2^{ix}—Sb1—Br1^{v}	147.72 (4)
Br1^{vii}—Sb1—Br1^{v}	34.243 (8)	Br2^{viii}—Sb1—Br2^{ix}	92.14 (8)
Br1^{iv}—Sb1—Br1^{v}	122.428 (18)	Br2—Sb1—Br2^{ix}	92.14 (8)

Br1^{iv}—Sb1—Br1^{vi}	88.18 (3)	Br2^{viii}—Sb1—Br2	92.14 (8)
Br2^{viii}—Sb1—Sb1^{i}	89.80 (4)	Sb1^{x}—Br1—Sb1^{i}	180.00 (4)
Br2^{viii}—Sb1—Sb1^{iii}	89.80 (4)	Sb1^{i}—Br1—Sb1^{ii}	34.243 (8)
Br2^{ix}—Sb1—Sb1^{iii}	89.80 (4)	Sb1^{x}—Br1—Sb1^{ii}	145.757 (8)

Symmetry codes: (i) −*x*+1, −*x*+*y*+1, −*z*+1; (ii) *x*−*y*+1, −*y*+1, −*z*+1; (iii) −*x*, −*y*+1, −*z*+1; (iv) −*x*+*y*−1, *y*−1, *z*; (v) *y*, −*x*+*y*+1, −*z*+1; (vi) *x*, *y*−1, *z*; (vii) −*y*+2, *x*−*y*+2, *z*; (viii) −*y*+1, *x*−*y*+1, *z*; (ix) −*x*+*y*, −*x*+1, *z*; (x) *x*, *y*+1, *z*.

Triformamidinium nonaiodididodiantimony (II)

Crystal data

$(CH_6N_2)_3[Sb_2I_9]$
M_r = 1421.63
Hexagonal, $P6_3/mmc$
a = 8.7552 (4) Å
c = 21.8474 (12) Å
V = 1450.32 (15) Å^3
Z = 2
$F(000)$ = 1194
D_x = 3.255 Mg m^{-3}
Mo $K\alpha$ radiation, λ = 0.71073 Å
Cell parameters from 5687 reflections
θ = 3.3–23.1°
μ = 11.42 mm^{-1}
T = 295 K
Prism, clear reddish red
0.13 × 0.13 × 0.09 mm

Data collection

Agilent SuperNova Dual Source diffractometer with a HyPix-Arc 100 detector
Radiation source: micro-focus sealed X-ray tube, SuperNova (Mo) X-ray Source
Mirror monochromator
Detector resolution: 10.0000 pixels mm^{-1}
ω scans
Absorption correction: multi-scan (CrysAlis PRO; Rigaku OD, 2022)
T_{min} = 0.263, T_{max} = 1.000
36967 measured reflections
896 independent reflections
456 reflections with $I > 2\sigma(I)$
R_{int} = 0.104
θ_{max} = 31.2°, θ_{min} = 3.3°
h = −12→12
k = −12→12
l = −30→31

Refinement

Refinement on F^2
Least-squares matrix: full
$R[F^2 > 2\sigma(F^2)]$ = 0.056
$wR(F^2)$ = 0.242
S = 1.05
896 reflections
19 parameters
1 restraint
Primary atom site location: dual
H-atom parameters not defined
$w = 1/[\sigma^2(F_o^2) + (0.1393P)^2]$ where $P = (F_o^2 + 2F_c^2)/3$
$(\Delta/\sigma)_{max}$ = 0.001
$\Delta\rho_{max}$ = 1.24 e Å^{-3}
$\Delta\rho_{min}$ = −0.44 e Å^{-3}

Special details

Geometry. All esds (except the esd in the dihedral angle between two l.s. planes) are estimated using the full covariance matrix. The cell esds are taken into account individually in the estimation of esds in distances, angles and torsion angles; correlations between esds in cell parameters are only used when they are defined by crystal symmetry. An approximate (isotropic) treatment of cell esds is used for estimating esds involving l.s. planes.

Refinement. Data was processed with the *CrysAlis PRO* software suite, and the structure was solved with *SHELXT* (Sheldrick, 2015*a*) and refined with *SHELXL* (Sheldrick, 2015*b*) within the *OLEX2* software suite (Dolomanov *et al.*, 2009).

Fractional atomic coordinates and isotropic or equivalent isotropic displacement parameters (Å^2)

	x	*y*	*z*	U_{iso}*/U_{eq}
Sb1	0.666667	0.333333	0.34472 (6)	0.0811 (7)

I1	0.50293 (8)	0.49707 (8)	0.250000	0.1046 (7)
I2	0.82616 (9)	0.65233 (18)	0.41593 (6)	0.1311 (7)
C1	0.333333	0.666667	0.407 (3)	0.20 (3)
C2	1.000000	1.000000	0.250000	0.20 (3)

Atomic displacement parameters (Å²)

	U^{11}	U^{22}	U^{33}	U^{12}	U^{13}	U^{23}
Sb1	0.0797 (8)	0.0797 (8)	0.0837 (10)	0.0399 (4)	0.000	0.000
I1	0.1107 (11)	0.1107 (11)	0.1240 (12)	0.0792 (10)	0.000	0.000
I2	0.1462 (11)	0.1093 (10)	0.1256 (11)	0.0547 (5)	−0.0190 (3)	−0.0380 (6)
C1	0.116 (18)	0.116 (18)	0.38 (7)	0.058 (9)	0.000	0.000
C2	0.20 (5)	0.20 (5)	0.19 (7)	0.10 (2)	0.000	0.000

Geometric parameters (Å, º)

Sb1—I1^{i}	3.2323 (12)	Sb1—I2^{iii}	2.8758 (13)
Sb1—I1^{ii}	3.2323 (12)	Sb1—I2	2.8759 (13)
Sb1—I1	3.2323 (12)	Sb1—I2^{iv}	2.8758 (13)
Sb1—I1^{iii}	3.2323 (12)	I1—I1^{ii}	0.0000 (13)
I1^{iii}—Sb1—I1^{i}	83.41 (3)	I2—Sb1—I1^{ii}	91.34 (3)
I1^{i}—Sb1—I1	83.41 (3)	I2^{iii}—Sb1—I1^{i}	91.34 (3)
I1^{iii}—Sb1—I1	83.41 (3)	I2^{iv}—Sb1—I1^{i}	91.34 (3)
I1^{iii}—Sb1—I1^{ii}	83.41 (3)	I2^{iii}—Sb1—I1	172.94 (5)
I1—Sb1—I1^{ii}	0.000 (18)	I2—Sb1—I1	91.34 (3)
I1^{i}—Sb1—I1^{ii}	83.41 (3)	I2^{iv}—Sb1—I1	91.34 (3)
I2^{iii}—Sb1—I1^{iii}	91.34 (3)	I2^{iii}—Sb1—I2	93.50 (5)
I2—Sb1—I1^{i}	172.94 (5)	I2^{iii}—Sb1—I2^{iv}	93.50 (5)
I2^{iv}—Sb1—I1^{ii}	91.34 (3)	I2^{iv}—Sb1—I2	93.50 (5)
I2^{iv}—Sb1—I1^{iii}	172.94 (5)	Sb1^{v}—I1—Sb1	79.62 (5)
I2^{iii}—Sb1—I1^{ii}	172.94 (5)	I1^{ii}—I1—Sb1^{v}	0 (10)
I2—Sb1—I1^{iii}	91.34 (3)	I1^{ii}—I1—Sb1	0 (10)

Symmetry codes: (i) *x*, *x*−*y*, *z*; (ii) −*y*+1, −*x*+1, −*z*+1/2; (iii) −*x*+*y*+1, −*x*+1, *z*; (iv) −*y*+1, *x*−*y*, *z*; (v) −*x*+*y*+1, *y*, −*z*+1/2.